REMOS - RECESSION MONITORING SYSTEM:
EXPERIMENT CONCEPT AND RESULTS OF THE FLIGHT ON REXUS 9

Christian Blank[1], **Hannah Boehrk**[2], **Marcel Duering**[1], **Serina Latzko**[1], **Uwe Sauter**[1], **Salome Schweikle**[1], **and Robert Wuseni**[1]

[1]*REMOS, info@remos-stuttgart.de*
[2]*DLR Institute of Structures- and Design Suttgart, Germany, hannah.boehrk@dlr.de*

ABSTRACT

REMOS stands for REcession MOnitoring System and is a student experiment launched on the REXUS 9 rocket in February 2011. The goal of the REMOS project is to develop a system enabling in-situ measurements of the thickness of ablative heat-shields of reentry vehicles by means of monitoring the material's electric properties. The system is tested during atmospheric reentry of the REXUS rocket in order to prove its applicability to future ablative thermal protection systems based on conductive materials. REMOS electronics are sensing resistance, capacitance and temperature in the probe sections. When probe material is ablated due to high thermal loads, the electrical properties of the probe sections change, thus providing temporal and spatial information on material thickness. Video data of three cameras is used for validation of the sensor data being stored and transmitted directly to the ground-station. The data gathered by the service-system's inertial measurement unit and GPS-receiver was evaluated to compute the inflow vector. In the present paper, the architecture and implementation of the REMOS flight experiment will be presented. The results from preflight tests, the launch campaign and post-flight analysis will be compared.

Key words: REMOS, DLR, REXUS, REXUS 9, TPS.

1. INTRODUCTION

Space vehicles require high-performance thermal protection systems (TPS) that provide high temperature insulation capability with low weight, high strength and reliable integration with the supporting structure. Damage or failure of TPS cannot be tolerated as its integrity before each launch and reentry is essential to the success of the mission. Consequently, knowledge of the heatshield recession is important for the design of new reentry vehicles in order to reduce life-cycle costs, to increase safety margins and to improve mission reliability. The goal of the REMOS project is to develop a system enabling real-time measurements of the thickness of ablative heatshields of reentry vehicles by means of monitoring the material's electric properties. It shall be tested during atmospheric reentry of the REXUS rocket in order to prove the system's applicability to future ablative TPS. The primary (p) and secondary (s) objectives of this experiment are:

- Measure electrical material characteristics. (p)
- Use video data for experiment verification. (p)
- Investigate the transferability to larger scales. (s)
- Gather video data for public relations usage. (s)

The REXUS rocket is a single-stage, spin-stabilised sounding rocket with a nominal diameter of 356 mm. It is capable of transporting a payload of 80 kg to an altitude of 90 km on a parabolic trajectory.

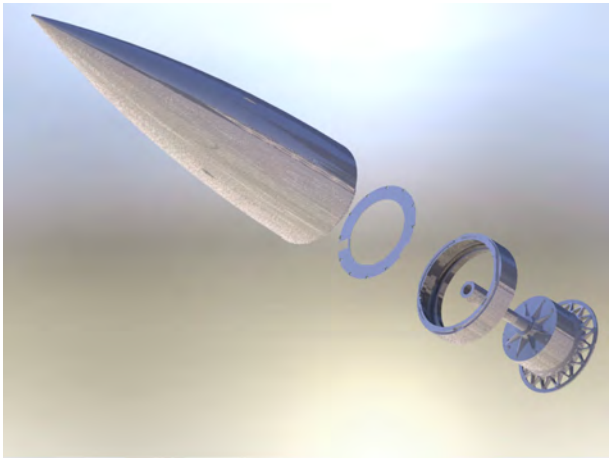

Figure 1. REXUS nosecone section

At the beginning of this document the flown trajectory and a method for the extraction of the direction of flow as well as the predicted in-flight temperatures will be described. Following, the basic idea of the measurement principle and the entire structural and electronial design of the experiment are introduced. Finally the measured and evaluated data is discussed and conclusions are derived.

2. MISSION

The experiment was on standby, protected by the nosecone during launch and activated 60 s after lift-off at an altitude of approximately 52 km. The cameras recorded the nosecone separation at an altitude of 62 km at t = 74 s. From this point the probe was exposed to the flow. The three measurement channels were activated shortly after reaching the apogee of 80.63 km at t = 138 s. The experiment shut down after 400 s before final descent on a parachute. The hot phase along with the maximum deceleration occurs during descent between 220 and 250 s after lift-off, as depicted in Figure 2.

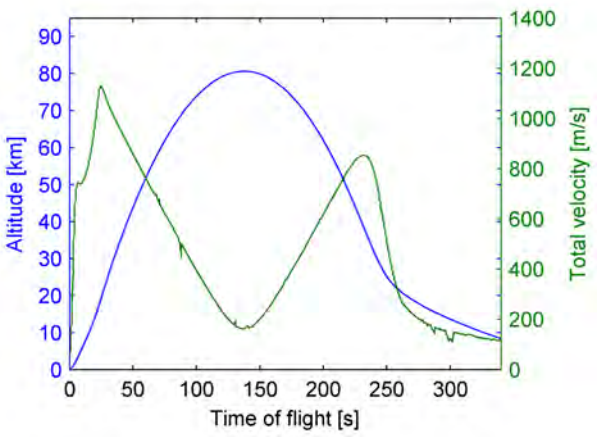

Figure 2. Altitude and total velocity over time

2.1. Determination of Inflow Direction

Among other data the REXUS Service Module provides GPS position data and data from the Inertial Measurement Unit (IMU). REMOS relies upon IMU data for the determination of inflow vector; altitude and velocity are determined using GPS data.

Coordinate System and Conventions

The REXUS 9 reference frame is based on a cartesian coordinate system whose X-axis defines the roll-axis of the rocket. It's Y-axis specifies the 0°-line of the perimeter while the Z-axis completes the coordinate system to be right-handed, as displayed in Figure 3.

The inflow direction is described by two angles: the in-plane angle α, which indicates the direction within the Y-Z-plane and the out-of-plane angle β. This angle shows the deviation from the plane and is positive when inclined towards the X-axis.

Calculation of angles α and β is done as follows:

$$\alpha = \begin{cases} \text{atan2}(a_z,\, a_y) & : \quad a_z >= 0 \\ 360° + \text{atan2}(a_z,\, a_y) & : \quad a_z < 0 \end{cases} \quad (1)$$

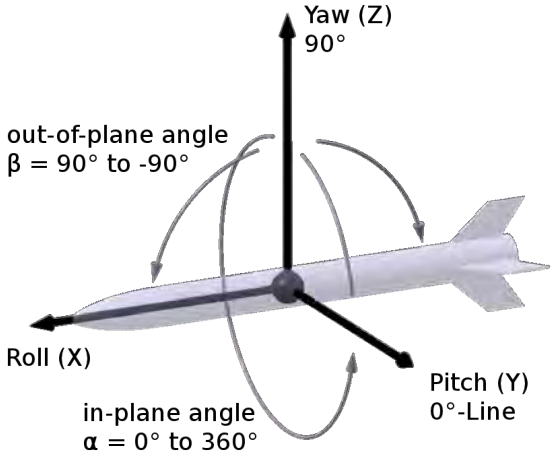

Figure 3. Body Frame Coordinate System

$$\beta = \text{atan2}\left(a_x,\, \sqrt{a_y^2 + a_z^2}\right) \quad (2)$$

where a_x, a_y and a_z are the accelerations measured in m/s^2.

2.2. Aerothermodynamics

On the tip of the REXUS 9 Rocket the REMOS experiment is directly exposed to the flow. During the supersonic phase of the launch, it is protected by the nosecone. After nosecone separation the thermal environment is cooling down to -100°C, but gas density is below $6{\cdot}10^{-5}$ kg/m^3 (p = 4 Pa) above 70 km resulting in negligible heat transfer due to convection. Heat is predominantly exchanged via thermal radiation. Coming from the apogee of 80.63 km, the total velocity increases to up to 854 m/s (Ma = 2.7; t = 232 s) during the hot phase in an altitude of 20 km. The calculated curves turn out to be a good guess for the actually measured temperature profile. For the originally assumed apogee of 100 km, higher velocities and resulting thermal loads would have been encountered (see Figure 5). The entire hot phase of the reentry is characterized by supersonic flow conditions: A detached shock forms in front of the experiment module. Assuming a flow from the side, the shock distance is a function of the probe radius. The fluid is decelerated to subsonic speed and the gas temperature increases. A map of the Mach number distribution is given in Figure 4. It is the result of a numerical simulation of the reentry flow around the experiment module. For orientation Figure 5 also contains the calculated gas temperatures T_{AS} after a normal adiabatic shock calculated from the flight data. Calculations for the probe temperature were done based on a semi-empirical heat flux model of Equation 3 by Tauber [3]

$$\dot{Q} = C * \rho^N * v^M \quad (3)$$

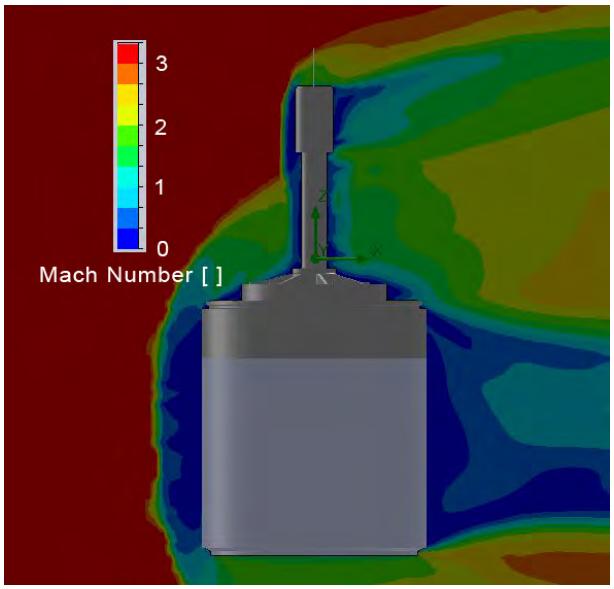

Figure 4. Map of the Mach number around the experiment module at an altitude of 20 *km*

with the heat flux $\dot{Q}$, the density ρ, the velocity v and the empirical constants C, N and M. Assuming a radiative heat exchange to thermal equilibrium this results in a first guess for the expected probe surface temperatures. Figure 5 shows that this temperature peaks at $T_{cRX80} = 267°\text{C}$ and $\dot{Q} = 3.6\,\text{kW/m}^2$ for the $80.63\,\text{km}$ apogee. For the originally assumed apogee at $100\,\text{km}$, a value of $T_{cRX100} = 439°\text{C}$ and $\dot{Q} = 11.5\,\text{kW/m}^2$ was calculated.

3. RECESSION MEASUREMENT

The goal of this experiment is to demonstrate the feasibility of an in-situ measurement system for ablative heatshield thickness. To reduce the amount of required modifications of existing designs, it was chosen to monitor electric properties of the heatshield material. This would reduce the required changes to the conditioning of its ohmic resistance, which can be achieved by changing the amount of uncombined carbon and/or other additives. This modification still allows for any shape, dimension and thicknesses of the heatshield tiles.
In the next section the theoretical background for such a heatshield material monitoring system is described. Since the REXUS flight only is suborbital and only reaches a fraction of the thermal loads of an orbital reentry, an appropriate material for the demonstrator has to be chosen, which is described after the introduction to the theory. Finally, the design process of the flight hardware is described briefly. This process was driven by requirements derived from the previously defined objectives and [1]. These requirements are grouped into four types. Altogether this resulted in

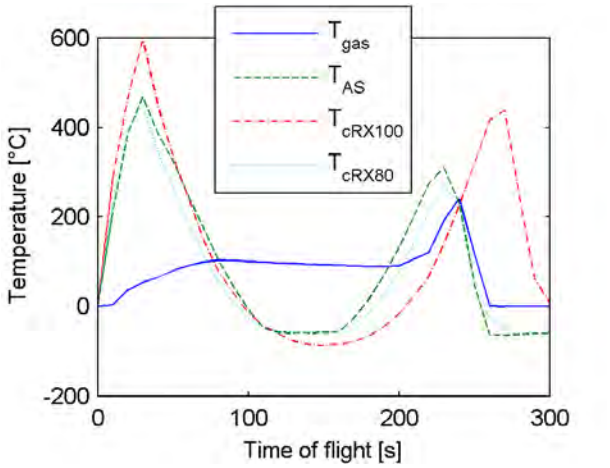

Figure 5. Calculated gas and probe surface temperatures as a function of the time of flight compared to the data recorded during the real flight

- 13 functional requirements
- 11 performance requirements
- 24 design requirements
- 10 operational requirements.

These requirements were used for verification in all phases of the systems engineering process.

3.1. Theory

The conductive foam probe material is attached to a substrate of fibre glass reinforced plastics (GFRP) on top of the aluminium boom. Four foam slabs form a single probe section. These slabs are interconnected by conduits, as shown in Figure 6. Between each of these foam

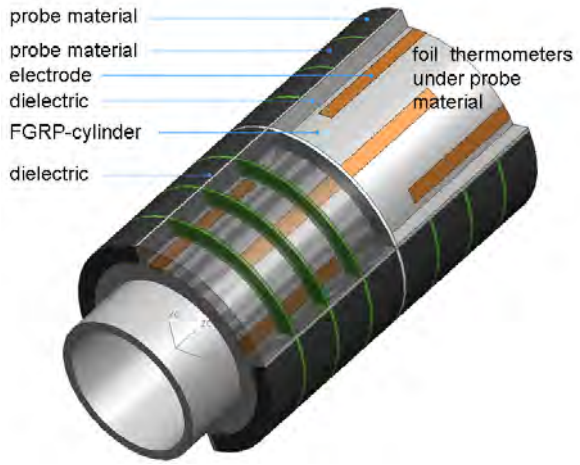

Figure 6. Probe Assembly

slabs there are thin ligaments of Kapton foil preventing

electric contact and serving as dielectric material (depicted in green in Figure 7). One Pt100 thermometer is

Figure 7. Measurement Principle

glued beneath each probe segment in order to measure the temperature of the foam elements. For ensuring contact between the foam and the measurement wires, the contacts are glued to the foam with conductive adhesive. The measurement connections are also glued to the copper contacts by conductive adhesive.
To monitor the change in capacitance and resistance of the probe two stripes of one foam square are connected on both ends. The two other stripes are responsible for the capacitance measurement. The two capacitors are connected in series to increase the capacitance. For the capacitance measurement eight wires are used while there are 16 wires for resistance and temperature measurements.
Every type of measurement is realized via a separately shielded harness so that the data logging isn't swayed. Each of the eight probe segments include the same connection structure. Three SUB-D 9 pole plugs were used for connecting the probe: one for the capacitance, one for the resistance, and one for the temperature measurement. Considering the predicted temperature profile (see Figure 5), an electrically conductive polyurethane foam was selected. The disintegration temperature for this material is below the expected peak temperature of 260°C.

3.2. Experiment Structure

The front section of REXUS 9 consists of the nosecone adapter and the nosecone itself. The usable space in this section of the REXUS rocket is limited by the following constrains:

- Due to required space for possible mounting of balancing masses, the maximum diameter is limited to 250 mm.
- The maximum usable height is limited to 500 mm by the separation mechanism in the ejectable nosecone.

An exploded view of all major parts can be seen in Figure 1. In addition to the geometric restrictions the experiment has to be designed to the requirements posed by the flightload envelope of the REXUS rocket. The foreseen procedure of verification in [1] is a random vibration test with the experiment operating as it will be during the actual launch. It is recommended to perform the test in all axes at the levels given in Table 1.

Table 1. Random Vibration Spectrum [1]

Axes	Frequency	Level	PSD
Longitudinal	20-2000	6.0	0.018
Lateral	20-2000	6.0	0.018
	Hz	g_{RMS}	g^2/Hz

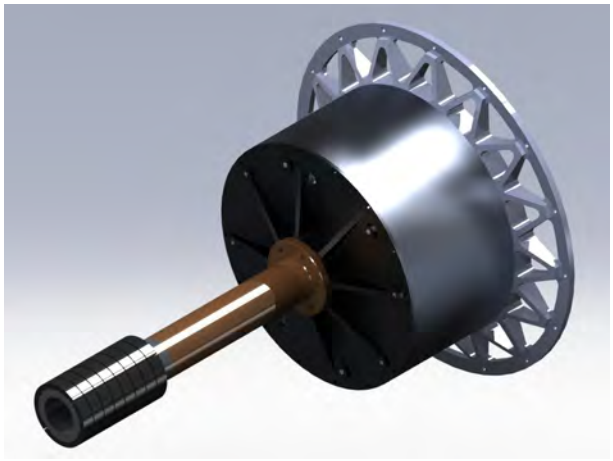

Figure 8. REMOS Experiment

As a result of the refinement of the systems engineering process the design shown in Figure 8 was developed. It shows the four major structural components of the experiment, which are described below in detail:

- The launch adapter bridges the gap between the REXUS interface and the inner cylinder. For reduction of mass it is designed as a truss structure.
- The inner cylinder serves as a spacer between the launch adaper and the cylinder cover. It's height is determined by the required space for the electronics boxes.
- The cylinder cover is the central structural part of the entire experiment. It provides interfaces for all required systems on the inward side and the mechanical interface to the sensor boom.
- The sensor boom is the supporting structure of the sensing elements, which are mounted onto a GFRP-pipe at the tip. It is mounted concentrical to the roll-axis of the rocket onto the cylinder cover. The length of the boom was limited by manufacturing capabilities. Although, it still is long enough, to provide

undisturbed flow conditions at the sensing elements (see Figure 4).

All supporting subsystems are mounted to the inward side of the cylinder cover with thermal insulating materials. It accommodates the central electronics box and two digital camera systems, one at each side of the box. The central focus for the entire structural design was the reduction of mass. An overall safety factor of $j = 1.5$ was selected. Due to limitations in manufacturing, requirements of electrical shielding and handling, this factor was overachieved at several locations.

During the early design phases the margins of safety were calculated analytically. In later design phases these calculations were supplemented by calculations with the finite element method (FEM). The applied load cases can be seen in Table 2.

Table 2. Load caseses for FEM

Load Case	Load	Origin
0	-	Eigenvalue calculation
1	56 g axial / 42 g lateral	Launch acceleration and 3 times vibration loads
2	7 g axial / 7 g lateral / 200° reentry	
3	6 g random x	Launch vibration
4	6 g random y	Launch vibration
5	6 g random z	Launch vibration

Load case 0 is not an actual load case, since only the systems eigenfrequencies and eigenmodes are calculated. These intermediate results provide a good reference for the following shaker test. As calculated by the FEM, the first vertical eigenmode appeared at $f_{v1} = 766$ Hz, the first lateral mode at $f_{l1} = 226$ Hz. Load case 1 was derived from the static flight loads plus three times the maximum dynamic loads occurring during the flight. This quasi-static load case primarily served for calculation of bolt forces. The random load cases were set up according to [1]. To confirm flight-readiness, a final shaker test with random loads at acceptance level was performed. The calculated eigenfrequencies could be confirmed with $f_{v1} = 550$ Hz, which represents a deviation of -28% and $f_{l1} = 190$ Hz, which represents a deviation of -16% to the FEM results. These deviations can be explained by the damping of the shaker adapter and the entire harness with its thermal insulation in the sensor boom, which had to be modeled in the FE-model as a distributed mass without damping.

3.3. Experiment Electronics

To fulfil the experiment's goals in terms of gathering flight data, the required electronic functionality can be summarised as follows:

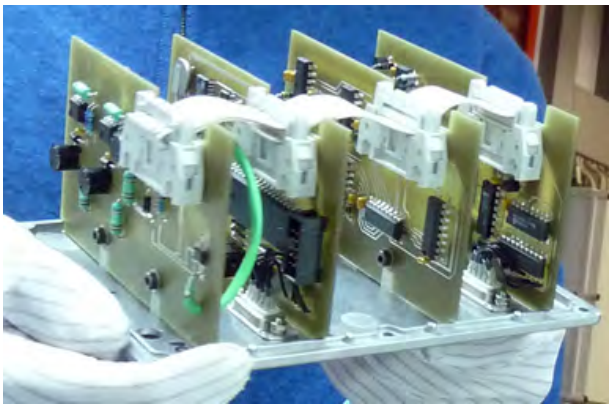

Figure 9. Electronics box

- Provide preconditioned power supply for the different systems of the experiment
- Sense resistances of the probe elements
- Sense capacitances of the probe elements
- Sense temperatures below the probe elements
- Sense temperature of the surrounding flow
- Store data onboard
- Transmit data via the service module to the ground station
- Record videos of the flight

The electronics are located in three aluminium enclosures to provide shielding from electromagnetic distortions. The smaller enclosures contain FlycamOne ECO cameras, which are used for imaging the probe during the flight. They provide sufficient time for recording onto microSD cards at VGA resolution, while weighing only 17 g. A third camera for direct TV downlink is installed in the nosecone adapter's cover.
The central electronics box accommodates four PCBs, each one dedicated to a specific task. These are power-conditioning and distribution (PCDU), onboard data handling (OBDH), capacitance measurement (C-SENSE) and resistance- and temperature measurement (RT-SENSE). Due to the special requirements, all PCBs were custom-built. The PCDU conditions the unregulated 28 V main-bus of the REXUS to an intermediate voltage by the use of a redundant configuration of two DC/DC-converters. For a better reduction of noise on the supply lines, the following continuous supply for the OBDH and the switchable supplies for the sensors and cameras are conditioned with linear regulators. The OBDH consists of an 8-bit Atmel RISC microcontroller (MCU) with a serial interface to a 16 Mbit FLASH storage, a real-time clock for synchronization, an RS422 interface to the REXUS service module and an interface to the sensing systems.

Table 3. Sensor characteristics of REMOS

Value	Type	Nr.	Range	Accuracy
		SENSORS		
T	Thermocouple	1	0 – 1024°C	± 0.5°C
T	Pt100	8	-50 – 300°C	± 0.2°C
R	Voltage divider	8	100 – 10^6 Ω	± 2.9 %
C	x556 timer	8	0.5 – 500 pF	± 0.05 pF
		HOUSEKEEPING		
T	KTY23-5	1	-50 – +150°C	± 0.3°C
V	Voltage divider	4	0 – 46 V	± 0.6 %

The capacitances of the probe elements are measured indirectly by using them to form triggerable single-pulse oscillators, whose wavelengths are used as a gating time for the OBDH's high-speed counter. The theoretical resolution of this system is 0.05 pF. The measurement of the resistances is done by simple voltage dividers, whose voltages are input to a 12bit ADC. The measurement of the temperatures is done by Pt100 sensors, which are supplied by constant current sources. The levels are amplified and fed to a second 12-bit ADC. A thermocouple in the tip of the sensor boom provides measurements of the temperature of the undisturbed flow. All measurements are done at a rate of 10 Hz. The entire system consumes less than 3.7 W of peak power (see Table 4).

The software, running on the MCU, is thread-oriented and was completely written in C. Depending on its operational mode, which is selected by hardwired timing signals from the RXSM, it takes care of the digitalisation of measurement data, their formatting for transmission and storage, as well as the processing of housekeeping data.

To confirm the functionality in the space environment a thermal-vacuum test was conducted. The entire experiment was placed in a vacuum chamber, where it was cooled down and heated up in the range of the qualification temperatures. Several simulations of an entire flight cycle were performed at different temperatures. Since a number of transmitters are operating next to the experiment in flight, it had to be confirmed, that these transmitters have no influence on the measurement system. This was accomplished by an electromagnetic interference test (EMI-test). As a result, small distortions of the signals were found in the frequency range of 150 MHz to 300 MHz. As these distortions stayed below 2% of the average measurement value and since the EMI-test was conducted at field strengths several magnitudes higher, than the expected values in flight, no distortions by the transmitters were expected.

Table 3 lists the measurement performance of REMOS. Constant deviations are given in the corresponding unit, quantity-dependant ones in %.

Table 4. Power characteristics of REMOS

Mode	Running systems	Consumption
Standby	housekeeping	1.46 W
Camera	+ cameras	3.36 W
Record	+ sensors	3.64 W

4. RESULTS

No major problems occurred during preparation of the flight. The experiment operated perfectly from power-up at t = −600 s to power-down at t = 600 s. The ground software operated as expected. Due to a switching problem only 7 s of analog video were transmitted to the control centre. Since the digital cameras recorded the preselected part of the flight, which could be secured after landing, the malfunction had no impact on the amount of usable video material. See Figure 10 for an example image from the video. Altogether, the experiment can be declared a success.

The following sections describe the in-flight performance of the system and present the measured temperature, resistance and capacitance results of the probe.

4.1. System Performance

The acquisition and transmission of all data worked as expected. The lost data packets during flight stayed below 5%, what was declared as an acceptable value for randomly distributed losses. The maximum amount of lost packets in series never exceeded 4 packages, what equals to 0.4 s. Although the outside temperature varied between -20°C at launch and +250°C at reentry, the electronics temperature only chilled down to +11°C and didn't exceed +14.5°C during flight. These values confirm, that a good thermal decoupling of the electronics box from the structure was achieved. All supply voltages stayed at their nominal values with less than 1% of varia-

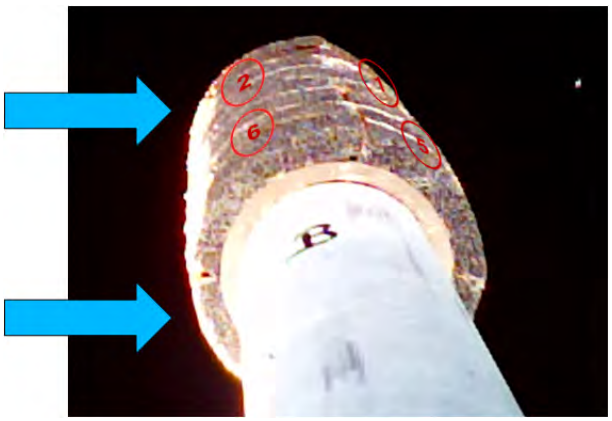

Figure 10. Image of the camera video looking at the boom with the probe

tion during switching of loads.

4.2. Attitude and inflow vector

Figure 11 shows the altitude and the total acceleration during t= 150 s upto 300 s. The total acceleration during the down-leg reaches $a_{total} = 0.2$ g at t = 220 s in an altitude of 48 km. This value is a reasonable choice to begin the analysis of the inflow vector.

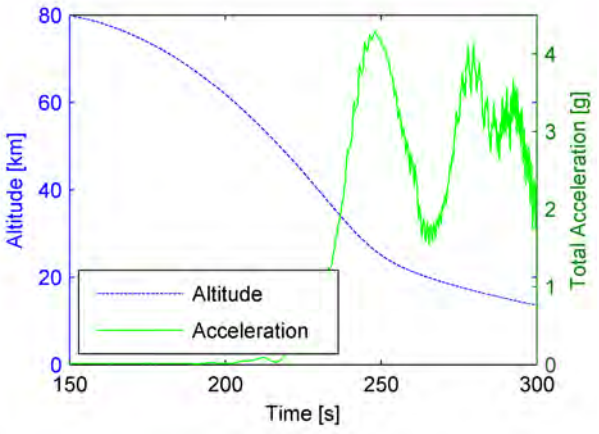

Figure 11. Altitude and total acceleration a_{total} at $t = 150s \ldots 300s$

After de-spin and nosecone seperation during ascent REXUS 9 begins an unstable tumbling movement. Athmospheric influence slows this tumbling down to a dynamically stable flat spin. The flat spin results in nutational movements which can be seen in a coupling of the in-plane and out-of-plane angle, depicted as shown in Figure 12. The oscillating inflow is reflected in the measurements of temperatures in individual probe sections.

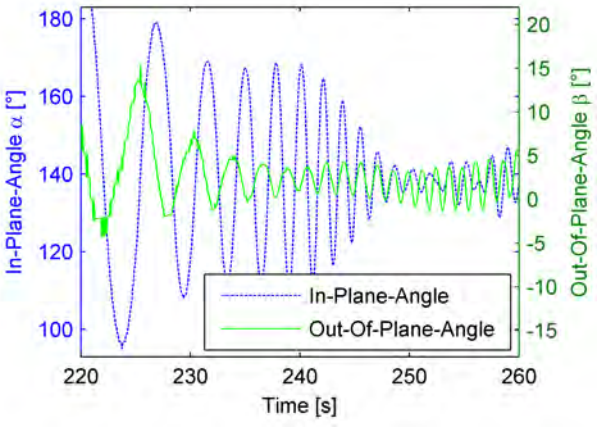

Figure 12. Coupling of α and β at $t = 220s \ldots 260s$

4.3. Flow Temperature

The ambient gas temperature T_{gas} was measured at the tip of the probe and during ascent it rose to 100°C due to the heat absorbed by the nosecone (Figure 5). After nosecone separation, the thermocouple is slightly cooling due to radiation but its thermal inertia is too big as to be able to measure the actual T_{gas} at altitudes above 60 km. During the hot phase, the value peaks at 241°C which is 35 K lower than the predicted surface probe temperature peak. Figure 4.3 shows the evolution of the

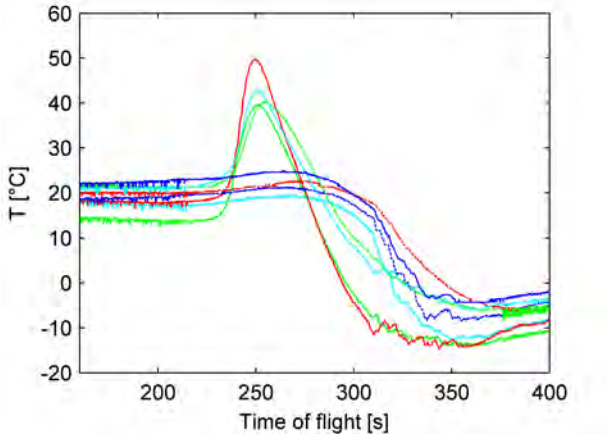

Figure 13. Temperatures measured under the 8 probe segments during reentry phase.

temperatures that were measured under each of the eight probe segments during the reentry phase. It is obvious that the probe segments in the direction of 80° and 173 ° are exposed to the highest heat flux. This is found for the segments in front as well as the ones in the back and confirming the observation that the flow is constantly coming from the 140° direction (see Figure 12). The segments on the opposite side are not even heated up entirely as gas density and consequently the heat flux is very low in the shadow of the probe. The peaks in probe segment temperatures are observed at t = 250 s; for T_{gas} this peak already occurs at t = 238 s. Looking at the amplitude of the peaks, one notes that the foam is a good thermal insulator and its thermal capacity is not negligible. Finding a suitable model for the average foam temperature based on these values remains an issue of investigation that is a prerequisite for eliminating the influence of the temperature on the resistance and capacitance measurements.

4.4. Capacitance and Resistance Data

The electrical properties, in particular the resistance and capacitance, for each channel are shown in Figure 4.4 and 4.4. The elements located in the direction of 80° and 173° (back and front) are effected by the flow, whereas the channels located on the downstream side are not af-

fected. The change is due to the increased temperature, which is predictable by Formula 4:

$$R = \rho(T)\frac{l}{A} \tag{4}$$

$\rho(T)$ is the density. The length l and the area A are geometric properties of each element. The fluctuating behaviour of the R channels correlates to the roll orientation and is not caused by signal noise. The measurement is highly sensitive to to mechanical influences. Here it acts as an indicator for the stagnation point. E.g. it can be used for detecting cracks in the material.

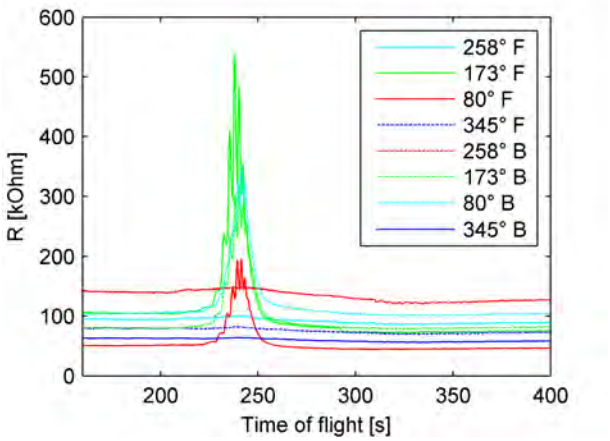

Figure 14. Measured data from resistance channels.

The magnitude of the change in capacitance differ from one channel to the other, since it also depends on the initial value. This is related to the manufacturing and the properties such as the thickness of the dielectric material and the size of the foam material vary for each channel.

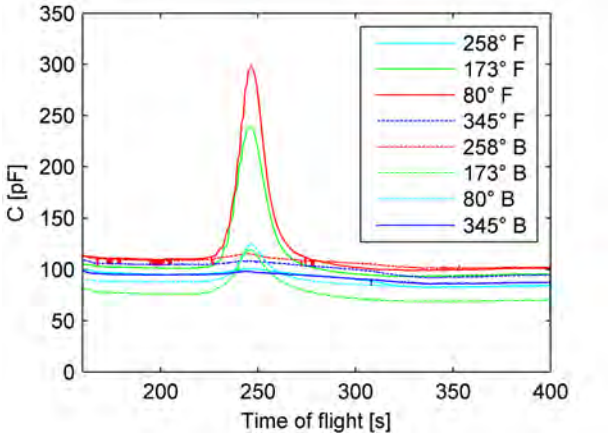

Figure 15. Measured data from capacitance channels

Looking at the values on the beginning of the measurement and at the final time, there is a shift, which is caused by modifications in the material. This was measured in previous tests on ground and verfied by the flight [4].

4.5. Conclusions & Outlook

The REMOS experiment for monitoring the electrical properties of an electrically conductive material operated flawlessly during the REXUS 9 flight. It turned out to be a reliable and space-proven system that can be integrated and operated at low cost and weight. Its design is modular and flexible: The probe can be exchanged and the measuring range allows for using it with other probe materials. The sampling rate of 10 Hz and the telemetry concept allow for realtime evaluation of the electric parameters. Complete and consistent data sets illustrating the changes in electric material properties as well as housekeeping data were recorded in the ground software. The temperature, resistance and capacitance values of the probe sections correlate well with the position data from the IMU. They have the potential to reveal the realtime state of the material. The system is thereby ready to be flown on rockets with higher apogees and other probe materials. A modular electronics system was developed and tested for a wide range of operation temperature, in vacuum conditions and under electromagnetic radiation. Its modules can be used for other applications, too.

ACKNOWLEDGEMENTS

We want to cordially thank the REXUS/BEXUS Program organizers and everyone involved. Furthermore, REMOS was supported by the DLR BK Stuttgart, ACME, Atmel, Bastler-Zentrale Stuttgart, Erich-Becker-Stiftung, Hostthenet, IEH, IRS, ITLR, Kucera, LBBW, Studentenwerk Stuttgart and Walter-Blohm-Stiftung.

REFERENCES

[1] EuroLaunch, 2009, REXUS User Manual v7.0

[2] RX09_11-02-10 REXUS-09 FRP

[3] M.E. Tauber et al.: Aerothermodynamics of Transatmospheric Vehicles. Journal of Aircraft, Vol. 24, September 1987

[4] Resistance and capacitance investigation of the probe material for REMOS DLR-IB 435-2010/32